Scientific
Research
Publishing

Laser Interferometer Based Measurement for Positioning Error Compensation in Cartesian Multi-Axis Systems

Y. Echerfaoui, A. El Ouafi, A. Chebak

Computer Science and Engineering Department, University of Quebec, Rimouski, Canada
Email: Abderrazak_elouafi@uqar.ca

Abstract

Accuracy is one of the most important key indices to evaluate multi-axis systems' (MAS's) characteristics and performances. The accuracy of MAS's such as machine tools, measuring machines and robots is adversely affected by various error sources, including geometric imperfections, thermal deformations, load effects, and dynamic disturbances. The increasing demand for higher dimensional accuracy in various industrial applications has created the need to develop cost-effective methods for enhancing the overall performance of these mechanisms. Improving the accuracy of a MAS by upgrading the physical structure would lead to an exponential increase in manufacturing costs without totally eliminating geometrical deviations and thermal deformations of MAS components. Hence, the idea of reducing MAS's error by a software-based alternative approach to provide real-time prediction and correction of geometric and thermally induced errors is considered a strategic step toward achieving the full potential of the MAS. This paper presents a structured approach designed to improve the accuracy of Cartesian MAS's through software error compensation. Four steps are required to develop and implement this approach: (i) measurement of error components using a multidimensional laser interferometer system, (ii) tridimensional volumetric error mapping using rigid body kinematics, (iii) volumetric error prediction via an artificial neural network model, and finally (iv) implementation of the on-line error compensation. An illustrative example using a bridge type coordinate measuring machine is presented.

1. Introduction

Current trends in precision engineering demand continually higher accuracy for various industrial applications. The multi-axis systems (MAS) are the basis of most production infrastructure ranging from machine tools to robotic applications, as well as for measurement equipment. The MAS performance in terms of accuracy is characterized by the moving accuracy of an open kinetic chain. The positioning accuracy is defined by the deviation between the programmed position and the actual tool position in the MAS workspace (cutting tools, probe or other end effectors). Errors in any relative motion on machine slides will result in a positioning error at the programmed position. Major contributors to inaccuracies in MAS's are quasi-static error sources, which are responsible for a very large proportion of the observed total deviation. They account for 70% of the volumetric error [1]. Quasi-static errors vary slowly with time and are related to stationary geometric errors resulting from manufacturing defects, misalignments due to assembly and installations, kinematic errors related to position control, and thermal errors associated with thermal distortion of the MAS components due to external heat sources. Other errors include dynamic errors resulting from control, software and deflections induced by vibrations and variations of internal forces. Obviously, these errors also have an important influence on the MAS accuracy. Moreover, whereas some error sources affect machine accuracy directly, others are interrelated with each other and their combined effects cause significant positioning errors. By considering all these diverse and variable error sources, one can understand the difficulties involved in improving MAS accuracy.

The traditional procedure for a relatively error-free MAS is to improve the design and manufacture of structural components. This approach is usually uneconomical since it leads to an exponential increase in manufacturing costs. An alternative approach using the concept of reducing error by compensation has proven to be more effective in upgrading MAS accuracy. Several studies have focused on enhancing the accuracy through on-line monitoring and computer error prediction and correction [2] [3] [4] [5] [6]. Various approaches based on quasi-static error analysis, modelling and compensation have been proposed over the last three decades. Some address the modelling problems of the final observed volumetric error in the MAS workspace by using empirical or analytical models [7]. Earlier studies have applied analytic geometry [1] and matrix error representation [8]. More recent reports describe the use of rigid body kinematics with homogeneous transformation matrices to model geometrical errors [9] [10] [11]. Unfortunately, the extensive experimental and analytical efforts required to build an accurate compensation procedure based on these models still hinder their commercial implementation. The approach proposed in this paper is based on an accuracy-monitoring scheme designed to improve the accuracy of multi-axis machines by compensating for geometric, thermal, load-induced and inertial errors. The essential feature of this monitoring system con-

sists of measuring and modelling the individual errors through an artificial neural network (ANN), combined with an improved multi-sensor fusion technique and a simplified kinematic synthesis model for time-variant and spatial-variant position error.

The paper presents a structured and comprehensive approach designed to improve the accuracy of Cartesian MAS's through software error compensation. Four steps are required to develop and implement this approach: (i) measurement of errors in six degrees of freedom along several profiles in each axis using a multidimensional laser interferometer measurement system, (ii) synthesis of tridimensional volumetric error mapping using rigid body kinematics, small angle approximations and homogeneous coordinate transformation, (iii) volumetric error prediction via an artificial neural network and kinematic models for on-line error compensation, and finally (iv) implementation of the on-line error compensation software package. The proposed approach is illustrated using a bridge-type touch probe coordinate measuring machine to demonstrate the effectiveness of the error compensation system. This paper also presents the approach's limitations and some other research ideas to overcome the difficulties that still obstruct this promising technology from being widely applied in various manufacturing systems.

2. Overview of MAS Errors

The accuracy of multi-axis systems is adversely affected by various error sources. Quasi-static errors including geometric, kinematic and thermal errors are accountable for a very large percentage of the observed total deviation. Geometric error is caused mainly by the MAS structural elements. It affects the repeatability of the MAS and its kinematic accuracy. It is also the direct measured error produced partially by other sources such as the thermal error. Kinematic error is a deviation manifesting in the ability of the MAS to reach the exact specified position. Position control of MAS slides, couplers, motors, etc. affect this error. Kinematic and geometric errors are interrelated. Thermal error is associated with thermal distortion and deformation of MAS structural components due to internal and external heat sources. Thermal error represents the largest source of MAS non-repeatability. The complex nonlinear nature of the thermal error variation makes it difficult to perform evaluation and analysis.

Figure 1 shows a typical structure of a prismatic joint in a Cartesian MAS axis. Each axis (X-axis) aggregates six error components associated with the prismatic joint's six degrees of freedom (dof): three translational errors in the x, y, and z directions (*i.e.*, linear displacement error $\delta_x(x)$, horizontal straightness error $\delta_y(x)$, and vertical straightness error $\delta_z(x)$, and three rotational errors about the x, y, and z axes (roll error $\varepsilon_x(x)$, yaw error $\varepsilon_y(x)$, and pitch error $\varepsilon_z(x)$). The lowercase term indicates the error direction and the term in parentheses indicates the moving slide. As an example, $\delta_y(x)$ refers to the straightness error in the Y direction when moving along the X-axis). Besides the six error components of
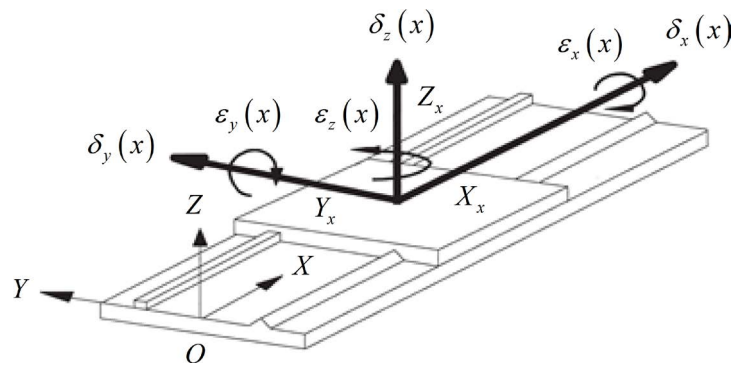
Figure 1. Schematic representation of error components associated with a prismatic joint in a Cartesian MAS.

each joint, there is also a perpendicularity or parallelism error between every two joints on MAS, S_{xy}, S_{yz} and S_{xz}. In the case of three-axis MAS, 21 errors are assessed and combined in order to synthetize the volumetric error components for the error compensation.

3. Errors Description and Modelling

The final errors between the actual and the desired MAS tool position can be calculated using kinematic modelling techniques. To derive the kinematics of a MAS with complex configurations, homogenous coordinate transformation techniques can be used. Cartesian MAS's are typically composed of a sequence of structural elements connected by joints that provide translational motion. Using Rigid Body Kinematics, each axis motion relative to the other axes and to the reference frame can be modelled using a Homogeneous Transformation Matrix (HTM). An HTM in tridimensional space is a 4×4 matrix. It can be used to represent one coordinate system with respect to another or with respect to the reference coordinate system (RCS). In this way, the location of the MAS tool is established relative to the RCS and the resultant volumetric error is estimated.

3.1. Geometric Errors Model of Linear Axis

An HTM describes the pure translation of an ideal axis (**Figure 1**) for the X-axis in the following form:

$$\left[{}^{R}T_{X} \right]_{ideal} = \begin{bmatrix} 1 & 0 & 0 & x \\ 0 & 1 & 0 & 0 \\ 0 & 0 & 1 & 0 \\ 0 & 0 & 0 & 1 \end{bmatrix} \tag{1}$$

where, x denotes the position of the X-axis coordinate system (O_x, X_x, Y_x, Z_x) with respect to the RCS (O, X_r, Y_r, Z_r). When taking the 6 dof error motion into account, the total error motion of the axis is a combination of rotational and translational errors. Using HTM and assuming small angular errors, the actual translation along a real X-axis is given by:

$$\left[{}^{RCS}T_X \right]_{actual} = \begin{bmatrix} 1 & -\varepsilon_z & \varepsilon_y & x+\delta_x \\ \varepsilon_z & 1 & -\varepsilon_x & \delta_y \\ \varepsilon_y & \varepsilon_x & 1 & \delta_z \\ 0 & 0 & 0 & 1 \end{bmatrix} \tag{2}$$

3.2. Geometric Errors Model of Three-Axis MAS

The positioning error is defined as the deviation between the actual and the desired MAS tool position. The actual position can be obtained by multiplying all of the HTMs with error components successively, going from the RCS to the tool coordinate frame. Similarly, the desired tool position can be obtained by multiplying all of the HTMs without error components successively, once again from the RCS to the tool coordinate frame.

Taking the Frame-XYZ type mechanism as an example, the schematic diagram of the structure of three-axis MAS and corresponding coordinate frames is illustrated in **Figure 2**. The HTM that can describe the spatial relationship between the RCS and the tool coordinate frame can be given as:

$$^{RCS}T_{tool} = {}^{RCS}T_X \times {}^{X}T_Y \times {}^{Y}T_Z \times {}^{Z}T_{tool} \tag{3}$$

The actual tool coordinates $P_a\,(x_a,\,y_a,\,z_a)$ in the RCS can be obtained by:

$$\begin{bmatrix} P_a & 1 \end{bmatrix}^{\mathrm{T}} = {}^{RCS}T_{tool} \times \begin{bmatrix} 0 & 0 & -L & 1 \end{bmatrix}^{\mathrm{T}} \tag{4}$$

where L is the tool dimension in Z direction.

The desired coordinates of the tool in the RCS, $P_d\,(x_d,\,y_d,\,z_d)$, can be obtained by setting the error components in Equation (3) to zero. The volumetric error vector $E\,(E_x\,E_y\,E_z)$ can be obtained by:
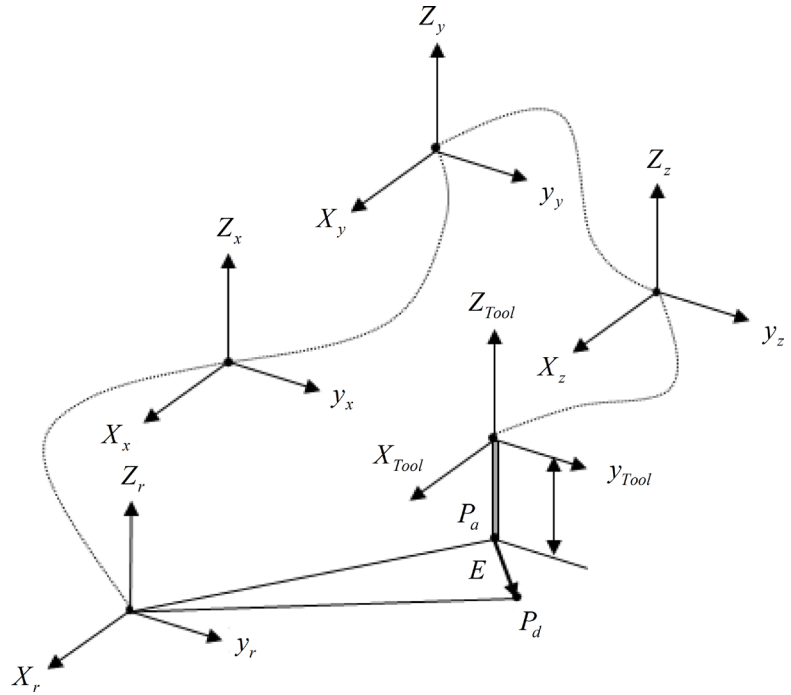

Figure 2. Volumetric error vector and coordinate frames of a typical 3 axis mechanism.

$$[E \quad 0]^T = [E_X \quad E_Y \quad E_Z \quad 0]^T \tag{5}$$

$$[E \quad 0]^T = [P_a \quad 1]^T - [P_d \quad 1]^T \tag{6}$$

The total volumetric error (E_v) illustrated in **Figure 2** can be computed by:

$$E_V = \sqrt{E_X^2 + E_Y^2 + E_Z^2} \tag{7}$$

4. Errors Measurements

The choice of the best error measurement method is essential for building an accurate and robust predictive model. Several measurement methods are well defined by existing standards and have been methodically tested and implemented by industry. These methods can be separated into two classes: indirect and direct. Indirect measurement methods involve measuring techniques which focus on superposed errors requiring multi-axis simultaneous movement [12]. These methods are developed as quick checks for an integral MAS test, giving an idea of the range of deviation. Indirect measurement methods use artefacts or standard references with known dimensions to measure the errors (calibrated artefacts, partially or totally non-calibrated artefacts, magnetic ball bars, double ball bars, special test pieces and other contour and displacement line measurements tests).

Indirect methods also use a few measuring tools from direct methods and apply them in different positions and orientations. Direct measurements are further classified into two classes based on the metrological reference used: material based methods using artefacts (*i.e.*, straightedges, scales or step gauges) as references, and laser-based methods using laser light propagation and its wavelength as a reference.

Laser-based methods are mainly used to evaluate errors of linear motion using a laser interferometer. As mentioned above, normal 6 dof geometric errors of a moving stage consist of the positioning error along the moving axis, two straightness errors perpendicular to the moving axis, and three angular errors along three perpendicular axes. The laser interferometers are commonly used to make extremely accurate measurements of linear displacement. The basic theory for laser interferometers dates back to the early 1900s with the Michelson Interferometer [13]. Modern interferometers are highly portable computer-controlled devices that are relatively easy to use and offer a wide range of data acquisition and analysis capabilities.

A laser interferometer uses a laser source emitting a focused, monochromatic light beam. In its basic configuration, the set-up includes a stationary light source, a beam splitter, a stationary reference reflective target, and a mobile reflective target, although there are several variants of laser interferometers. The simplest and the most popular ones can perform measurements in only one axis to measure linear and angular displacements, flatness, etc. For example, 1D interferometers characterized by a greater linear measurement accuracy of ±0.5 μm/m are available through many manufacturers. In order to evaluate the volu-

metric error by means of a 1D laser, it is necessary to rearrange the laser head and the optics many times in each axis being measured. In addition, the measuring system must be recalibrated after each reconfiguration and the measurements need to be repeated at least 3 to 5 times. This means that it would take a few days to determine the 21 components of the geometric error for a 6 dof MAS.

The 3D version interferometers are designed based on 1D interferometer with added optoelectronic circuits enabling the simultaneous measurement of the lateral motions of the reflector. Linear errors, horizontal straightness and vertical straightness along a given axis are evaluated at the same time. The 6D version interferometers are built by adding more optoelectronic circuits. Errors associated with the 6 dof along a moving axis are measured simultaneously. With the 6D interferometers, the measuring time can be substantially reduced (60% - 75%) [14]. The 6D laser setup needs to be executed only once for each of the axes measured.

Among the multidimensional laser measurement systems available, the XD Laser series manufactured by Automated Precision Inc. (API) provides simultaneous measurement of all axis errors from a single setup. The 6D system also features the ability to evaluate velocity, acceleration, parallelism, squareness, and flatness. **Figure 3** shows the configuration of a high-precision XD laser model consisting of a laser head, an interferometer module, and a sensor head and a laser controller. The XD laser system is a Helium Neon laser operating at a frequency of 473 THz with 0.6329 μm wavelength.

The laser head emits a highly stabilized and collimated laser beam that is aligned with the axis being measured. The laser beam is split into three paths, one for the vertical and horizontal straightness measurements, one for the angular measurements, and one for linear distance measurement. The straightness and angular measurements are achieved with precision optics and a lateral effect photo-detector [15]. **Figure 4(a)** highlights the internal structure of the laser receiver, configured for linear error measurements requiring both the interfero-
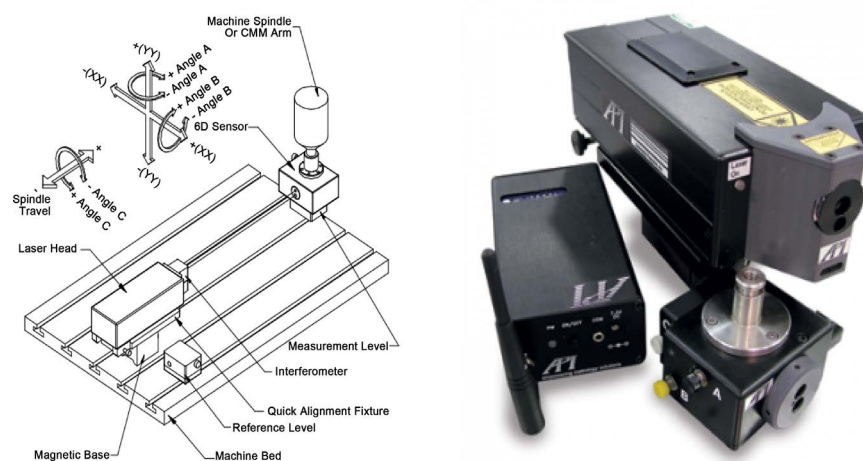

Figure 3. Volumetric error vector overall view of the 6D XD laser system [15].
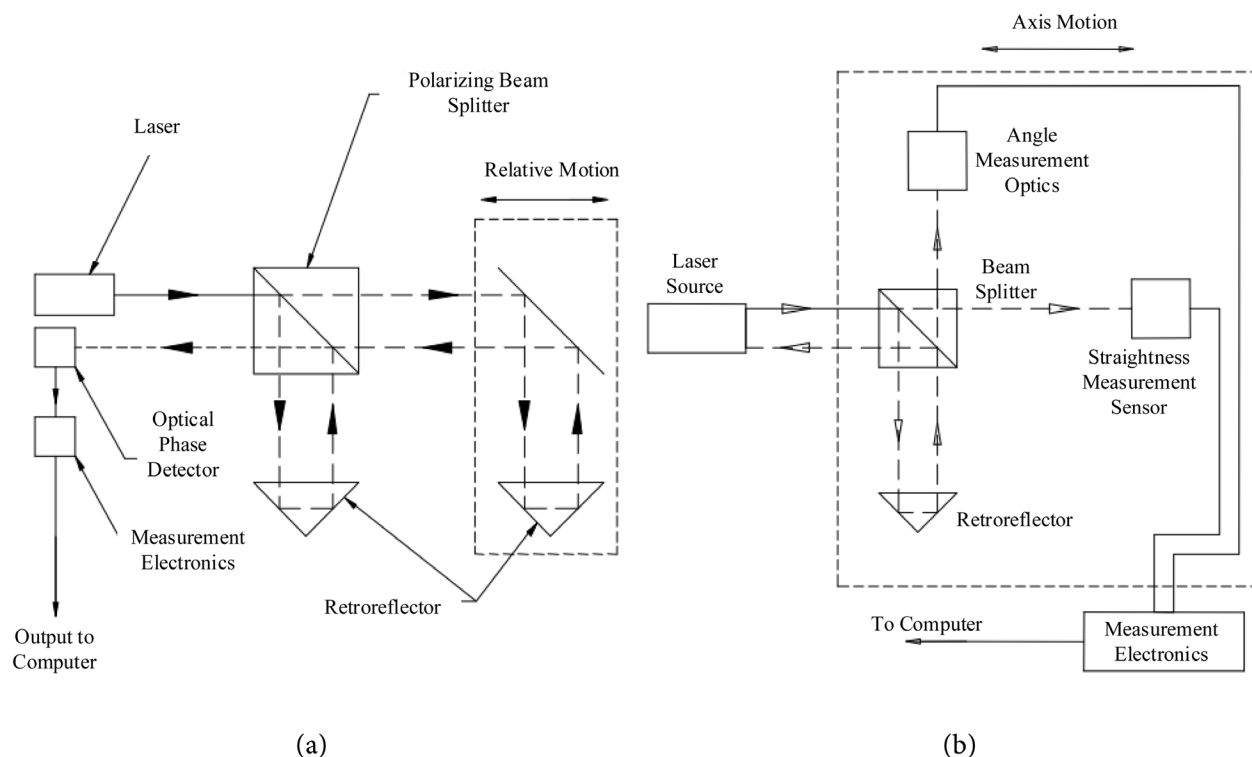
Figure 4. Simplified block diagram of the laser system receiver used for: (a) linear measurements and (b) angular measurements [15].

meter and retro reflectors. **Figure 4(b)** illustrates the laser receiver configuration for straightness and angular measurements. In this case, the laser beams are sent from the beam splitter to the angle measurement optics, working as a miniature autocollimator, and to straightness sensor.

5. Application in the Case of a Coordinate Measuring Machine

Coordinate Measuring Machines (CMMs) are widely used in industry to inspect the dimensional and geometric characteristics of complex and high-precision parts. A common but inadequate industrial practice is to assume any part measurement to be nearly error free, or in the worst case to be within CMM volumetric error specifications provided by the CMM manufacturer or by calibration. This oversimplification of CMM precision is often misleading since other factors are involved. Indeed, CMM precision strongly depends on inaccuracies induced by various error sources.

Deviations of the mechanical structure resulting from geometric imperfections, static forces and thermally induced strains are commonly recognized as the largest contributors to the total measurement error. The results reported in the literature indicate a typical geometric ranging between 5 and 40 μm and a thermal effect of 8 to 15 μm/˚C·m for commonly used CMMs. The errors introduced by the probing system can deteriorate the performance of the CMM by about 1 to 10 μm overall.

As the necessity to improve the working accuracy of CMMs is well recognized, the question then arises as to the best way to achieve it. It is clear from the literature that the CMM structural error dominates. It is thus natural to begin the investigation and development of a compensation system assessing this problem.

The proposed CMM error compensation system operates using the encoder positions *X*, *Y* and *Z* triggered as the probe tip hits the inspected part, and returns the compensation E_x, E_y and E_z that must be added to the encoder position in order to improve machine position accuracy. ANNs and kinematic models provide the compensation vector as a function of the encoder positions. The compensated position is then used as input to the CMM software for geometric computation and metrological analysis. This compensation system is built and implemented on a moving bridge CMM equipped with a Renishaw head and probing system. The CMM workspace is $400 \times 400 \times 400$ mm along, respectively, the *X*, *Y* and *Z* axes.

The steps required to build the error compensation model comprise: (i) the measurement of three error components along several *X*, *Y* and *Z* profiles using a multidimensional laser interferometer system, (ii) the building of the neural network models that estimate the geometric errors anywhere within the CMM workspace, (iii) the construction of the predicted volumetric error components using a kinematic model, and finally (iv) the implementation and validation of the error compensation software package. As the CMM is a three-axis MAS, a total of 21 errors are to be assessed and combined in order to evaluate the volumetric error components for error compensation. Table 1 presents an error budget providing the potential errors within the CMM workspace.

The schematic diagram of the structure of the CMM and the corresponding coordinate frames is illustrated in Figure 5. Based on this configuration, the spatial relationship between the reference coordinate frames and the tool coordinate frame is established using a homogeneous transformation matrix. This relationship can be obtained using Equation (3).

By setting the offsets between the coordinate frames of adjacent axes to zero and by neglecting the higher order infinitesimal terms, the volumetric error components can be expressed as:

$$E_X = \delta_x(x) + \delta_x(y) + \delta_x(z) - y\left[\varepsilon_z(x) + S_{xy}\right] + z\left[\varepsilon_y(x) + \varepsilon_y(y) - S_{xz}\right] \\ + L\left[\varepsilon_y(x) + \varepsilon_y(y) + \varepsilon_y(z)\right] \tag{8a}$$

$$E_Y = \delta_y(x) + \delta_y(y) + \delta_y(z) - z\left[\varepsilon_x(x) + \varepsilon_x(y) + S_{yz}\right] - L\left[\varepsilon_x(x) + \varepsilon_x(y) + \varepsilon_x(z)\right] \tag{8b}$$

Table 1. Summary of geometrical errors in the CMM.

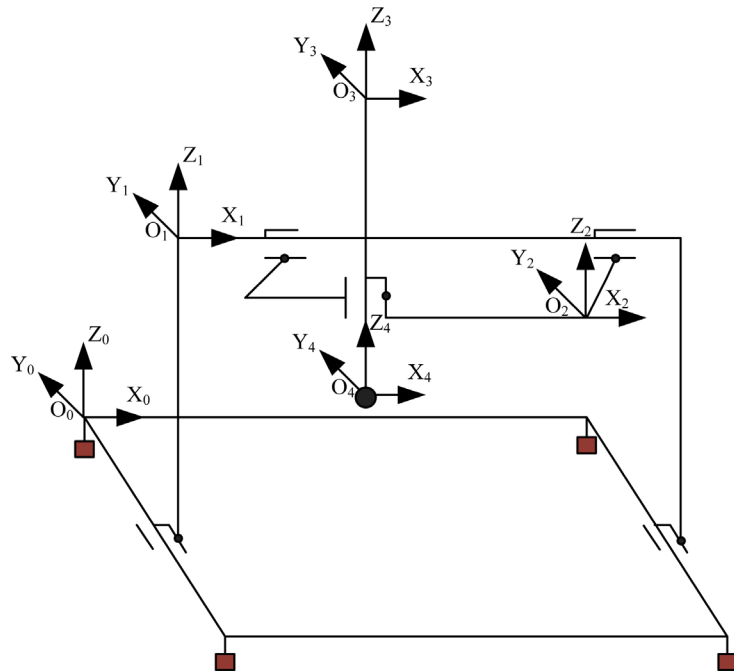| Axis	Translation component			Rotational component			Orthogonality
X	$\delta_x(x)$	$\delta_y(x)$	$\delta_z(x)$	$\varepsilon_x(x)$	$\varepsilon_y(x)$	$\varepsilon_z(x)$	S_{xy}
Y	$\delta_x(y)$	$\delta_y(y)$	$\delta_z(y)$	$\varepsilon_x(y)$	$\varepsilon_y(y)$	$\varepsilon_z(y)$	S_{yz}
Z	$\delta_x(z)$	$\delta_y(z)$	$\delta_z(z)$	$\varepsilon_x(z)$	$\varepsilon_y(z)$	$\varepsilon_z(z)$	S_{xz}

Figure 5. Coordinate frames of the CMM under investigation.

$$E_Z = \delta_z(x) + \delta_z(y) + \delta_z(z) + y\varepsilon_x(x) \tag{8c}$$

5.1. Errors Measurement Procedure

To measure the displacement errors over the travel ranges of three CMM slides, an API XD laser interferometer system is used. Table 2 presents a simplified picture of the laser interferometer system characteristics. The experimental setup is presented in Figure 6. Measurements are carried out in a controlled temperature environment within a tolerance of ±1˚C at displacement intervals D_x, D_y and D_z of 400 mm. The measurements are performed using the minimum speed in order eliminate dynamic effects and determine the most accurate geometrical deviation.

The results of the geometrical error measurements, illustrated in Figures 7-9, show that the linear displacement errors are larger than the specified CMM accuracy of ±2 µm (7 µm, 10 µm and 8 µm respectively for X, Y and Z axis). The maximum straightness errors vary on average between 10 µm and 12 µm depending on the measured axis. Finally, pitch, yaw and roll errors measured at the same positions are similarly presented. The maximum angular errors average between 7 and 10 arcsec.

After the various individual geometric errors are measured, the positioning volumetric error components (ME_x, ME_y and ME_z) are synthesized using the kinematic model presented in Equation (5). Figure 10 illustrates the spatial-variant error components in X-Y, Y-Z and X-Z planes. Maximum errors without compensation reach 35, 30 and 25 µm in X, Y and Z directions, respectively.

Table 2. 6-D brief review of the laser interferometer characteristics [15].

Accuracy	Options		
	Regular	Precision	High Precision
Linear (ppm)	0.5	0.2	0.2
Linear Range (m)	25	25	-
Straightness (μm)	±(1.0 + 0.2/m)	±(0.5 + 0.1/m)	±(0.2 + 0.05/m)
Max. range (μm)	± 500	±300	±100
Pitch and Yaw (arcsec)	±(1.0 + 0.1/m)	±(0.5 + 0.5/m)	±(0.2 + 0.05/m)
Max. Range (arcsec)	±800	±400	±50
Roll (arcsec)	±1.0	±0.5	±0.5
Squareness (arcsec)	±1	±0.5	±0.5
Temperature (°C)	0.2	0.1	0.1
Humidity (%)	5	3	3
Pressure (mmHg)	1	0.3	0.3
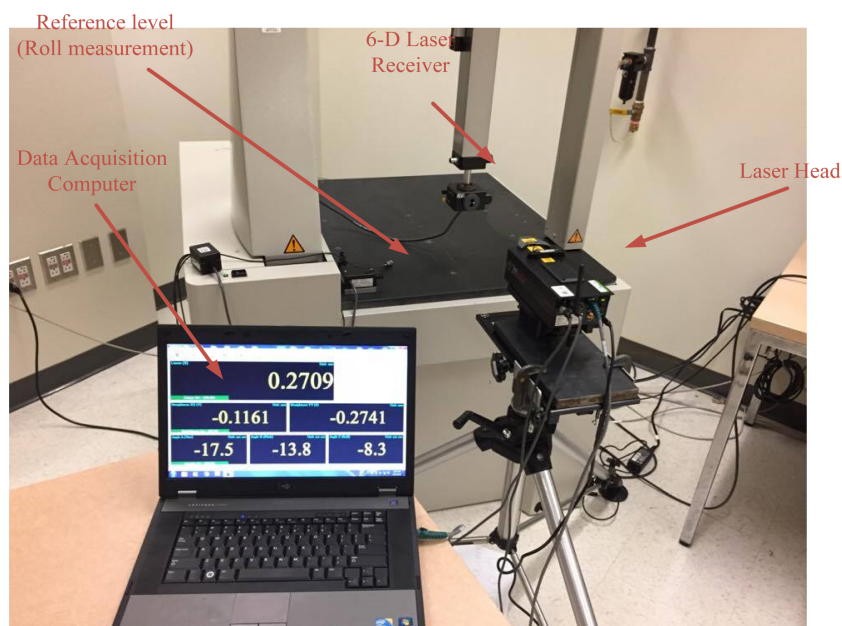
Figure 6. Measurements setup.
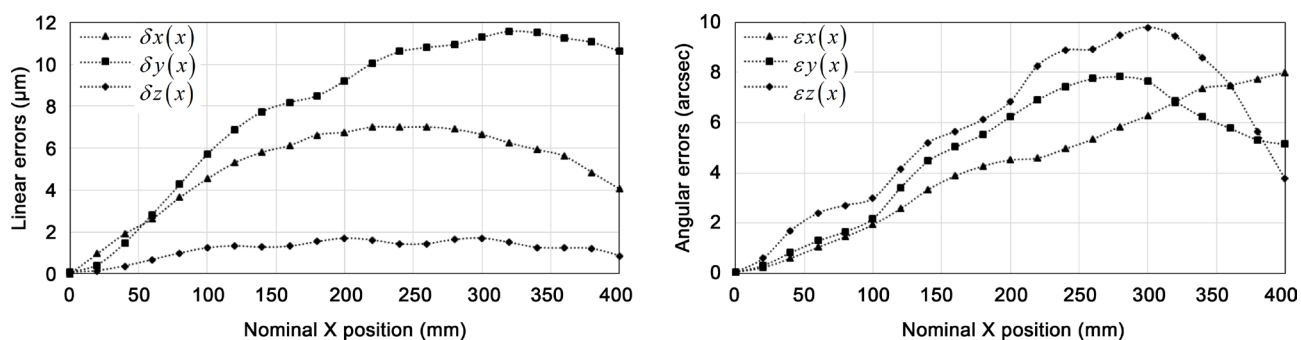
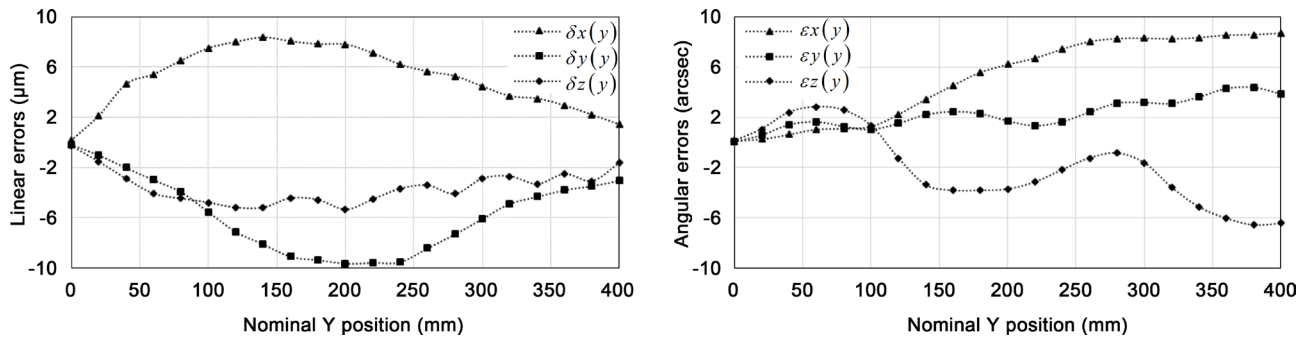**Figure 7.** Measured geometric errors for X-displacement.

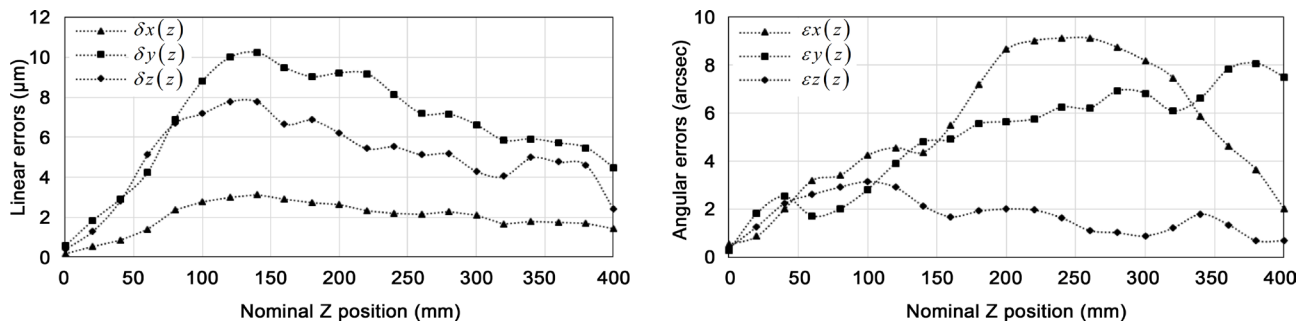**Figure 8.** Measured geometric errors for Y-displacement.

Figure 9. Measured geometric errors for Z-displacement.
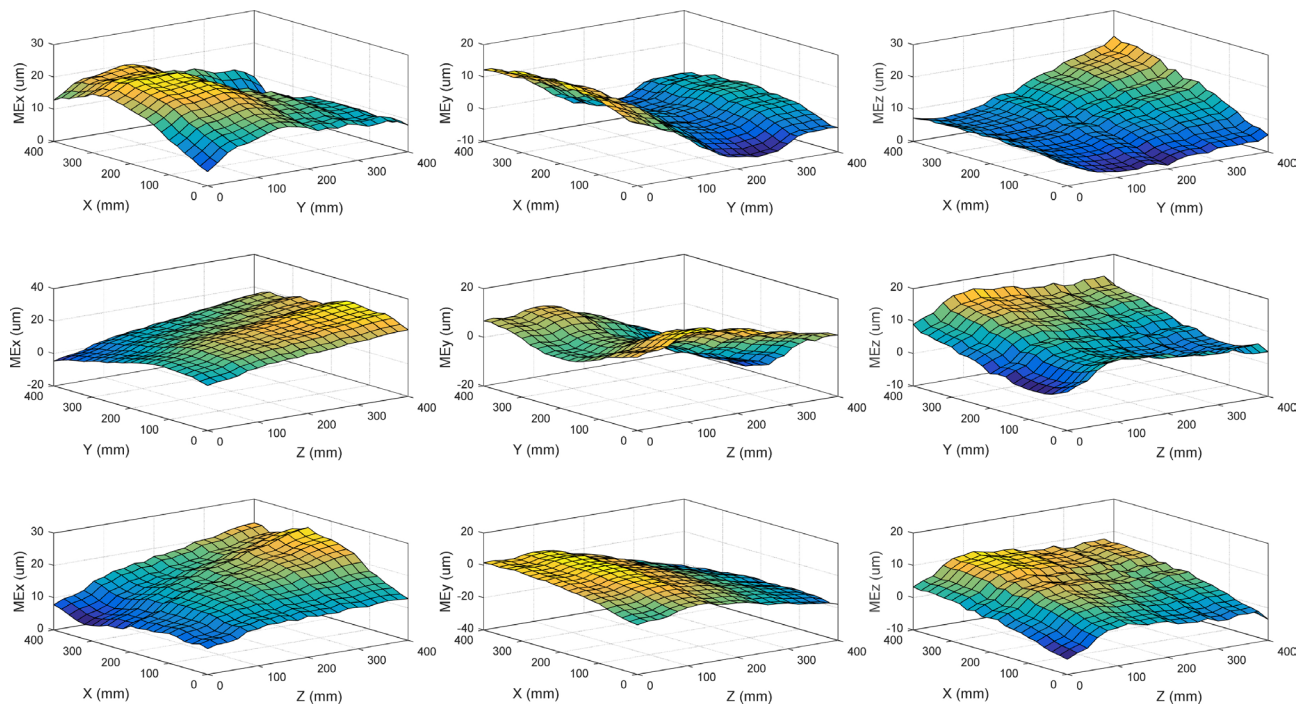

Figure 10. Measured 3D volumetric error components for the XYZ workspace.

5.2. Artificial Neural Network Modeling

In order to evaluate the volumetric error at any location on the CMM workspace, a set of error components must be predicted using a pre-established empirical model. For the bridge-type CMM, the volumetric error components can

be considered as a combination of the 21 geometric errors. The difficulties of modeling lie in the fact that the components of the error are highly nonlinear and strongly correlated to the 3D coordinates in the CMM workspace. Therefore, the empirical model must be multiple-input multiple-output nonlinear model. Hence, an ANN model is proposed to predict six error components for each axis. Because the three orthogonalities are assumed to be constant, they are not considered in the prediction models.

While various ANN techniques can be used in this approach, a multilayer feed-forward neural network seems to be one of the most appropriate options because of its simplicity and flexibility [16] [17]. As shown in **Figure 11**, a neural network consists of N neurons, which are each connected to the neurons of the adjacent layers. A threshold value $\theta_{,l}$ is associated with each neuron. The output of each neuron is determined by the level of the input signal in relation to the threshold value. These signals are modified by the connection weights $W_{i,j,c}$ (also called synaptic strengths) between the neurons.

Let $I_{j,l}$ be the input to the jth neuron on layer l, then the output of this neuron is given by:

$$O_{j,l} = \frac{1}{1+\exp\left(-I_{j,l}+\theta_{j,l}\right)} \tag{8}$$

where,

$$I_{j,l} = \sum_{i=1}^{n_l-1} W_{i,j,l} O_{j,l-1} \tag{9}$$

where $O_{i,l-1}$ is the output of the ith processing neuron of layer l-1, n_{l-1} is the number of neurons on layer l-1, and $W_{i,j,l}$ is the weight of the connection between neuron i on layer l-1 and neuron j on layer l.

The ANN structure shown in **Figure 11** provides a typical and useful example to illustrate the mechanism of the supervised learning process. In response to a
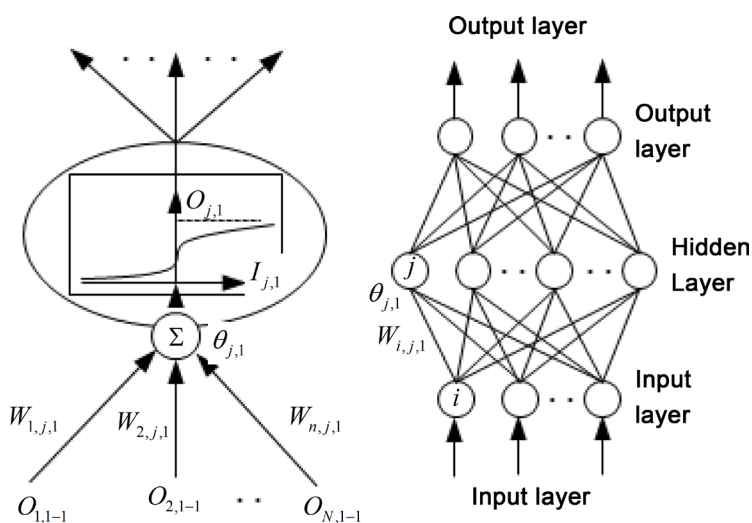

Figure 11. Simple computational elements of the multiplayer feed-forward neural network.

pattern presented to the input layer, the ANN attempts to produce an associated pattern by its output layer. The hidden layers are employed to reject noises that are present in the input signals, so that the task of feature extraction can be performed effectively. So far as the training of the multilayer feed-forward neural network is concerned, the algorithm most widely used is known as error back-propagation (also known as the generalized delta rule). In this rule, the network parameters are adapted from one iteration to another using the following equations:

$$W_{i,j,l}(n+1) = W_{i,j,l}(n) + \eta \delta_{j,l} O_{i,l-1} + \alpha \left[W_{i,j,l}(n) - W_{i,j,l}(n-1) \right] \quad (10)$$

$$\theta_{j,l}(n+1) = \theta_{j,l}(n) + \eta \delta_{j,l} + \alpha \left[\theta_{j,l}(n) - \theta_{j,l}(n-1) \right] \quad (11)$$

where,

$$\delta_{j,l} = \left(dO_{j,l} - O_{j,ll} \right) O_{j,ll} \left(1 - O_{j,ll} \right) \text{ if } l = ll \quad (12)$$

$$\delta_{j,l} = O_{j,l} \left(1 - O_{j,ll} \right) \sum_{k} \delta_{k,l+1} W_{j,k,l+1} \text{ if } l < ll \quad (13)$$

where, $dO_{j,e}$ is the desired output from the jth output of the network using the eth training exemplar. The gain η, and momentum α, can take values between 0 and 1 providing settings for the learning rate and filters for high-frequency variations of the error surface. The exemplar values input in the network are linearly mapped between 0 and 1 range. The network outputs will allow values between 0 and 1 which can be mapped back to full range.

Three multilayer feed-forward neural network are proposed to fit the experimental measurements. That means all the 18 error components are predicted using only three ANN models, which significantly saves time for modelling. Before training the ANN models, it was important to establish the size of the hidden layer and optimize the training performances. It is known that too few hidden processing neuron will not train the ANN well. However, too many hidden processing neuron will increase the difficulty of training and the ANN will try to model everything including the noise.

In order to optimize the ANN architecture, the idea is to approximate the relationship between the size of the hidden layer and the complexity of the relationship between dependent and independent modelling variables. For this evaluation, 4 network architectures were studied: $[(i)^x(i+1)^x(o)]$, $[(i)^x(2i + 1)^x(o)]$, $[(i)^x(i + 1)^x(2i + 1)^x(o)]$ and $[(i)^x(2i + 1)^x(3i + 1)^x(o)]$, where (i) and (o) are the number of inputs and outputs respectively. Training mean square error (MSE_t), validation mean square error (MSE_v) and the total mean square error (MSE_{tot}) are used as modelling performance criteria for choosing the best ANN architectures. The evaluation of the produced models is based on the three validation procedures summarized in **Table 3**. The best results are achieved using the $[(i)^x(2i + 1)^x(o)]$ ANN. Consequently, this network structure is selected.

Globally, the modelling results present good agreement between measured and predicted error components in training and validation phases. The three ANN prediction models present excellent performances with an average error of

Table 3. Validation procedures.

Procedures	Training	Validation
VP$_1$	100% of data	100% of data
VP$_2$	50% of data picked randomly	Remaining data (50%)
VP$_3$	Data acquired under specific positions	Remaining data
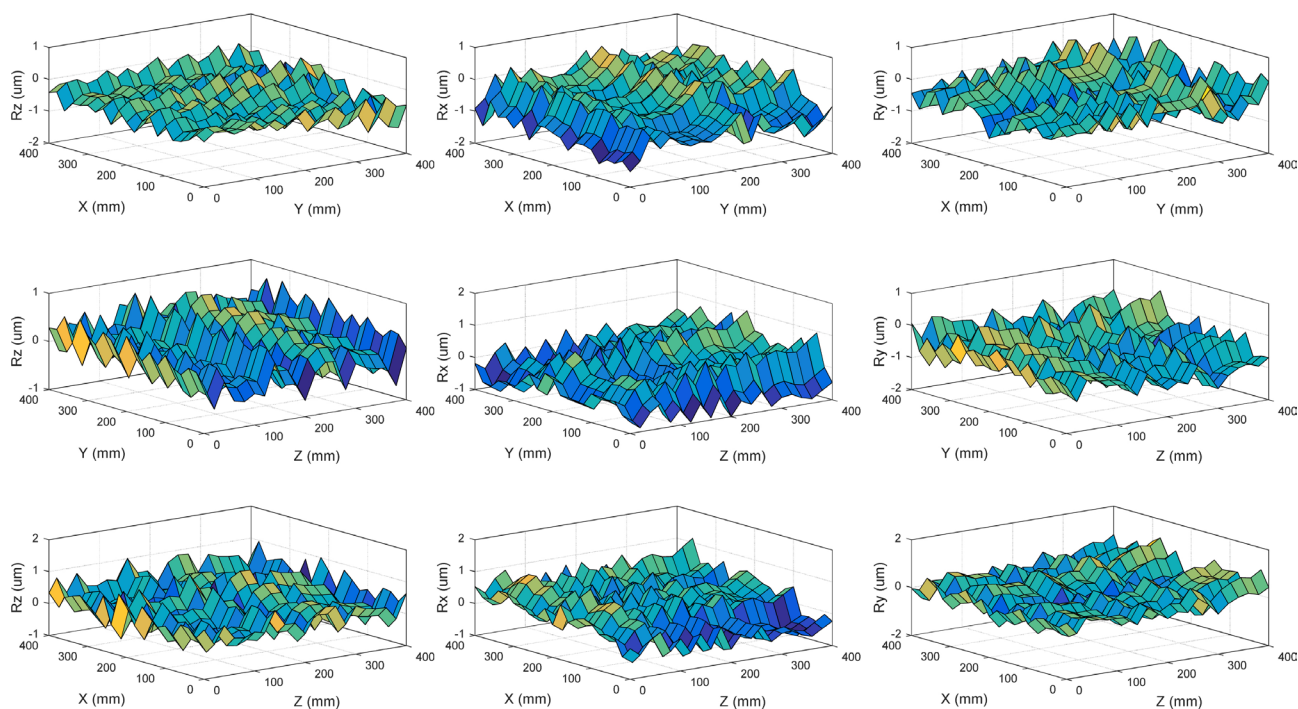
Figure 12. Residual errors representing the differences between measured and predicted 3D volumetric error components for the XYZ workspace.

less than 5% for the 18 error components.

As soon as the ANN models are built producing the error components, predicted positioning volumetric error components (PE_x, PE_y and PE_z) are synthesized using the kinematic model established in Equation (5) and the compensation values are generated. Simulation tests conducted using various conditions demonstrate the effectiveness of the proposed error prediction and compensation approach. **Figure 12** visualizes the residual errors (R_x, R_y and R_z) representing the differences between the measured and the predicted tridimensional spatial-variant errors in the *xy*, *yz* and *xz* planes. The prediction errors are relatively small and do not exceed 6 μm out of a total volumetric error of more than 63 μm. From these results, it is clear that the proposed error compensation approach can improve the volumetric working tolerance of the CMM by reducing more than 90% of the quasi-static errors.

5.3. Error Compensation

The error compensation system operates using the encoder positions *X*, *Y* and *Z* triggered as the probe tip hits the inspected part, and returns the compensation

E_x, E_y and E_z that must be added to the encoder position in order to improve machine position accuracy. The ANN model provides the error components as a function of the encoder positions. Volumetric error components are synthesized using the kinematic model. The compensated position is then used as an input to the CMM software for the geometric computations and metrological analysis.

In order to evaluate the performance of the error identification and compensation approach, a diagonal test is designed. In this test, the CMM is controlled to move from the RCS position along the volumetric diagonal. The travel distance along the diagonal is 692.82 mm. The machine is controlled to move by 69.282 mm constant steps along the diagonal (40 mm on each axis simultaneously at a constant measuring speed). At each position, the current coordinates from the CMM controller are collected and transferred to the computer where the errors are synthesized. The actual and predicted distances are then compared, and the correction of the diagonal travel distance is applied. The actual and predicted diagonal distances as well as the residual errors are presented in **Figure 13**. As can be seen in the graph, from volumetric errors exceeding 27 μm (7, 23 and 12 μm, respectively, in the *x*, *y* and *z* directions), the maximum residual error is lower than ±2 μm. Though obtained under conditions minimizing random errors by collecting data under the most stable conditions possible, these results indicate that the proposed error identification approach can produce an efficient active error compensation of the systematic errors, thereby leading to significant improvement of the MAS accuracy. When working at the micrometer level, other errors like probing system error, metrology software errors, and especially dynamic errors must also be addressed.

6. Conclusions

In response to the increasing demand for higher quality, improving the accuracy of multi-axis systems through software error compensation is becoming increasingly important in modern manufacturing. The success of such methods de-
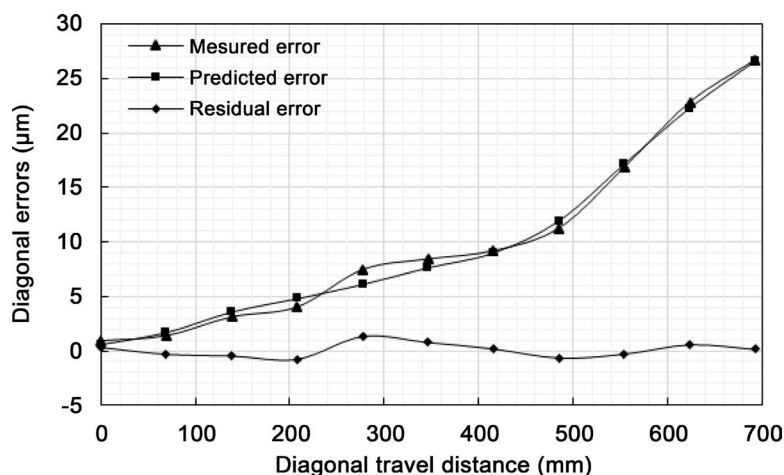

Figure 13. Residual error representing the difference between measured and predicted diagonal distances.

pends on the degree of consistency in identifying error sources, the precision of the measurement techniques, the reliability of the modelling approach, and its robustness in evaluating the error components at any location within the MAS workspace. Applicable to a MAS of diverse configurations, the proposed laser interferometer based measurement and ANN predictive modelling approaches are built step-by-step to satisfy these requirements.

This paper presents a structured and comprehensive method designed to improve the accuracy of a Cartesian MAS through software error compensation. The proposed method is based on the measurement of error components using an accurate multidimensional laser interferometer system, on the 3D volumetric error mapping using rigid body kinematics and a homogeneous transformation matrix, and on ANN predictive modelling. Implemented on a bridge-type coordinate measuring machine, the proposed compensation approach improves the MAS accuracy by reducing more than 90% of the quasi-static errors, thus dropping the maximum volumetric error from 63 μm to fewer than 6 μm. Nonetheless, it is important to mention that all of the tests were performed at very low velocities. This suggests that the errors could be much greater if the MAS is operating at high velocities, due to dynamics.

References

[1] Eman, K., Wu, B., and DeVries, M. (1987) A Generalized Geometric Error Model for Multi-Axis Machines. *CIRP Annals-Manufacturing Technology*, **36**, 253-256. https://doi.org/10.1016/S0007-8506(07)62598-0

[2] Lee, J.H., Liu, Y., and Yang S.H. (2006) Accuracy Improvement of Miniaturized Machine Tool: Geometric Error Modeling and Compensation. *International Journal of Machine Tools and Manufacture*, **46**, 1508-1516. https://doi.org/10.1016/j.ijmachtools.2005.09.004

[3] Ahn, K.G. and Cho, D.W. (2000) An Analysis of the Volumetric Error Uncertainty of a Three-Axis Machine Tool by Beta Distribution. *International Journal of Machine Tools and Manufacture*, **40**, 2235-2248. https://doi.org/10.1016/S0890-6955(00)00048-1

[4] Okafor, A. and Ertekin, Y.M. (2000) Derivation of Machine Tool Error Models and Error Compensation Procedure for Three Axes Vertical Machining Center Using Rigid Body Kinematics. *International Journal of Machine Tools and Manufacture*, **40**, 1199-1213. https://doi.org/10.1016/S0890-6955(99)00105-4

[5] Zhu, S., *et al.* (2012) Integrated Geometric Error Modeling, Identification and Compensation of CNC Machine Tools. *International Journal of Machine Tools and Manufacture*, **52**, 24-29. https://doi.org/10.1016/j.ijmachtools.2011.08.011

[6] Rahman, M., Heikkala, J. and Lappalainen, K. (2000) Modeling, Measurement and Error Compensation of Multi-Axis Machine Tools. Part I: Theory. *International Journal of Machine Tools and Manufacture*, **40**, 1535-1546. https://doi.org/10.1016/S0890-6955(99)00101-7

[7] Ramesh, R., Mannan, M. and Poo, A. (2000) Error compensation in machine tools—a review: part I: geometric, cutting-force induced and fixture-dependent errors. *International Journal of Machine Tools and Manufacture*, **40**, 1235-1256. https://doi.org/10.1016/S0890-6955(00)00009-2

[8] Slocum, A.H. (1992) Precision Machine Design. Society of Manufacturing Engineers, Dearborn, MI, USA.

[9] Srivastava, A., Veldhuis, S. and Elbestawit, M. (1995) Modelling Geometric and Thermal Errors in a Five-Axis CNC Machine Tool. *International Journal of Machine Tools and Manufacture*, **35**, 1321-1337. https://doi.org/10.1016/0890-6955(94)00048-O

[10] Sartori, S. and Zhang, G. (1995) Geometric Error Measurement and Compensation of Machines. *CIRP Annals-Manufacturing Technology*, **44**, 599-609. https://doi.org/10.1016/S0007-8506(07)60507-1

[11] Kiridena, V. and Ferreira, P. (1993) Mapping the Effects of Positioning Errors on the Volumetric Accuracy of Five-Axis CNC Machine Tools. *International Journal of Machine Tools and Manufacture*, **33**, 417-437.

[12] Schwenke, H., *et al.* (2008) Geometric Error Measurement and Compensation of Machines—An Update. C*IRP Annals-Manufacturing Technology*, **57**, 660-675.

[13] Michelson, A.A. and Morley, E.W. (1887) On the Relative Motion of the Earth and of the Luminiferous Ether. S*idereal Messenger*, **6**, 306-310. https://doi.org/10.2475/ajs.s3-34.203.333

[14] Lau, K., *et al.* (1999) An Advanced 6-Degree-of-Freedom Laser System for Quick CNC Machine and CMM Error Mapping and Compensation. *WIT Transactions on Engineering Sciences*, **23**, 421-434.

[15] Automated Precision I. (2010) User Manual XD LASER.

[16] Huang, S.H. and Zhang, H.C. (1994) Artificial Neural Networks in Manufacturing: Concepts, Applications, and Perspectives. *IEEE Transactions on Components, Packaging, and Manufacturing Technology*, **17**, 212-228. https://doi.org/10.1109/95.296402

[17] Meireles, M.R., Almeida, P.E. and Simões, M.G. (2003) A Comprehensive Review for Industrial Applicability of Artificial Neural Networks. I*EEE Transactions on Industrial Electronics*, **50**, 585-601. https://doi.org/10.1109/TIE.2003.812470